Theoretical Studies of Structure and Dynamics of Molten Salts: The LiF–ThF 4 System

ARTICLE *in* THE JOURNAL OF PHYSICAL CHEMISTRY B · OCTOBER 2014

Impact Factor: 3.3 · DOI: 10.1021/jp509425p · Source: PubMed

6 AUTHORS, INCLUDING:

W H Eugen Schwarz

Universität Siegen

199 PUBLICATIONS **3,854** CITATIONS

SEE PROFILE

Jun Li

Tsinghua University

283 PUBLICATIONS **8,929** CITATIONS

SEE PROFILE

THE JOURNAL OF PHYSICAL CHEMISTRY B

Article

pubs.acs.org/JPCB

Theoretical Studies of Structure and Dynamics of Molten Salts: The LiF−ThF_4 System

Jian-Biao Liu,[†,‡] Xin Chen,[†] Yi-Heng Qiu,[†] Chao-Fei Xu,[†] W. H. Eugen Schwarz,[†,§] and Jun Li*[,†]

[†]Department of Chemistry and Key Laboratory of Organic Optoelectronics and Molecular Engineering of the Ministry of Education, Tsinghua University, Beijing 100084, China

[‡]College of Chemistry, Chemical Engineering and Materials Science, Shandong Normal University, Jinan 250014, China

Supporting Information

ABSTRACT: LiF−ThF_4 molten salt (MS) is the fuel for advanced MS reactors. Knowledge of the microscopic MS structure and dynamics is required for an understanding of the macroscopic physical and chemical properties of the MS phases. We have performed molecular dynamics simulations on LiF−ThF_4 MS at different molar percentages (LiF/ThF_4 = 20.0 to 0.5) and temperatures (1100 to 1400 K). Experimental deductions and recent theoretical results on the coordination structures and transport properties of the MS are well reproduced. The density of states of the $[ThF_8]^{4-}$ species and the character of the Th−F bonding are investigated. The interplay between the microscopic structures and the dynamical properties is elucidated. Corresponding to the smaller effective radius of Zr, the activation barrier of the M^{4+}−F^- dissociation and the lifetime of the first coordination shell of M^{4+} are both smaller for M = Th than for M = Zr in the respective LiF−MF_4 systems. The shorter Zr−F bond is stronger than the longer Th−F bond, while the coordination number of the predominant $[ZrF_7]^{3-}$ species is smaller than that of the dominant $[ThF_8]^{4-}$ species. An approximate formula is proposed for the lifetime of F^- ions in the first solvation shell of molten MF_n (M = Y, Zr, Th) in terms of the radial distribution function.

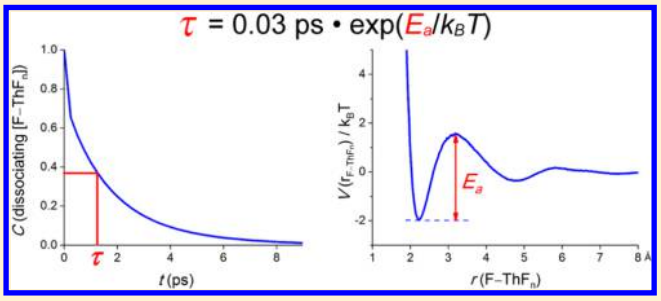

1. INTRODUCTION

Molten salts (MS) are liquid mixtures of ionic species, typically at higher temperatures. Their chemical and physical properties strongly depend on the anions (e.g., monovalent F^- and Cl^-, divalent O^{2-}, etc.).[1] Despite the aggressive behavior of molten fluorides, they are of great practical interest in various industrial processes, including metallurgy, nuclear waste treatment, fuels, and coolants in advanced nuclear reactors.[2−6] Many studies of the physicochemical and electrochemical properties of molten fluorides have been carried out.[1,7−25] Interest in MS reactors has recently risen because of their safety and efficiency advantages.[26,27] Different kinds of salt mixtures containing ThF_4 and UF_4 dissolved in NaF, LiF, and/or BeF_2 have been proposed for MS reactors.[6,28]

The LiF−ThF_4 system is of particular interest as the base in the MS fast reactor.[6,28] A better knowledge of the *macroscopic* physical and chemical parameters in wide concentration and temperature ranges is required before industrial application, concerning heat transfer in the reactor, online fuel processing, and waste separation.[22,24,29,30] Further, the knowledge of the *microscopic* structures and dynamics in MS systems is required for the correct interpretation of the various spectroscopic data of MS species. Owing to the high temperature and corrosion difficulties in MS experiments and the vast number of mixing ratios, computational molecular dynamics (MD) simulations have proven as a very useful tool.[7,8,16−20] Effective pair-potentials between the ions are now known at the *ab initio* level, and they have been tested against various types of experimental data on MS with good agreement.[7,8,16−20,31,32]

In 2013, Dewan et al. had systematically studied the thermodynamic and transport properties of LiF−ThF_4 at the eutectic composition (78 mol % LiF, 22 mol % ThF_4) at a range of temperatures by using MD simulations.[19] Very recently, Salanne et al. have comprehensively reviewed the composition and temperature variation of various thermophysical properties of LiF−ThF_4 MS systems.[33] We here report similar MD calculations with particular emphasis on the relationship between microscopic structures, structural dynamics, and macroscopic properties, the character of Th−F bonding, and the nuclear magnetic resonance (NMR) parameters. The calculation details are communicated in section 2. The results from *ab initio* calculations on selected molecular clusters and MD simulations of the MS are presented and discussed in section 3. Our conclusions are summarized in section 4.

2. THEORETICAL METHODS

The MD simulations were performed for molten LiF−ThF_4 at 1200 K and different molar compositions x (x_{ThF_4} from 0.05 to

Received: October 31, 2014
Published: October 31, 2014

0.67) using the FIST module of the CP2K package.[34] The LiF−ThF_4 mixture at x_{ThF_4} = 0.5 was further studied at temperatures T = 1100 K to 1400 K (the upper half of the range covered by Salanne et al.).[33]

The applied interaction potential derives from the polarizable ion model,[31,32]

$$V(\mathbf{r}_{ij}) = V_{q-q} + V_{q-\mu} + V_{\mu-\mu} + V_{rep} + V_{disp}$$

where V_{q-q} means the ionic point-charge Coulomb interaction, $V_{q-\mu}$ is the point-charge induced-point-dipole interaction, $V_{\mu-\mu}$ is the dipole−dipole interaction, V_{rep} is the dominantly repulsive (Born-type) overlap repulsion, and V_{disp} is the C_6 + C_8 dispersion attraction. The singularities in the power terms of $V_{q-\mu}$ and V_{disp} were damped by exponential Tang−Toennies-type factors. The potential parameters were taken from Dewan et al.,[19] as listed in Table S1 of the Supporting Information. The systems were first equilibrated in a cube for 500 ps in the isothermal-isobaric (NPT) ensemble at a target pressure of 1 atm, and then further relaxed in the canonical (NVT) ensemble for 100 ps. The MD simulations were then run for 3000 ps. The time step used in the MD simulations was 0.5 fs. The particle numbers together with the obtained number densities are listed in Table 1.

Table 1. Molar Percentages of ThF_4 (x), Particle Numbers (N) in the MD Simulations, and Obtained Number Densities (in Å^{-3}) at 1 atm and 1200 K

x_{ThF_4}(%)	$N_{Th^{4+}}$	N_{Li^+}	N_{F^-}	N_{total}	number densities
4.85	11	216	260	487	0.0772
12.02	19	139	215	373	0.0743
19.88	33	133	265	431	0.0715
30.05	58	135	367	560	0.0677
40.00	54	81	297	432	0.0654
50.00	58	58	290	406	0.0632
66.67	58	29	261	348	0.0614

Quantum chemical calculations of the ionic clusters were performed using density functional theory (DFT), as implemented in the ADF-2013 package.[35] We used the generalized gradient approximation of the PBE exchange-correlation potential.[36] The atomic core orbitals [$1s^2$−$4f^{14}$] of Th and [$1s^2$] of F and Li were taken as frozen from numerical atomic Dirac−Fock−Slater calculations. The scalar relativistic zero-order regular approximation (SR-ZORA)[37,38] was applied for the extended valence Hamiltonian of the clusters. Slater-type basis sets of triple-ζ plus two polarization (TZ2P) quality were used for all atoms.[39]

3. RESULTS AND DISCUSSION

3.1. Ionic Radial Distribution Functions. We studied the average spatial configurations of the ion clusters in MS with the help of the radial distribution function (RDF) $g_{ij}(r)$ of ions j around the reference ion i. The g-functions for the pairs Th^{4+}−F^-, Li^+−F^-, and Th^{4+}−Th^{4+}, Li^+−Li^+, Th^{4+}−Li^+, and F^-−F^- at 1200 K are presented in Figure 1, for two different mole fractions (x_{ThF_4} = 0.12 and 0.67). The most frequent counterionic Th−F distance corresponding to the first peak of $g_{Th-F}(r)$ is near 2.24 Å, varying hardly with the concentration. Dewan et al.[19] had obtained 2.26 Å for x_{ThF_4} = 0.22, agreeing within 1% with our values. As shown in Table 2,

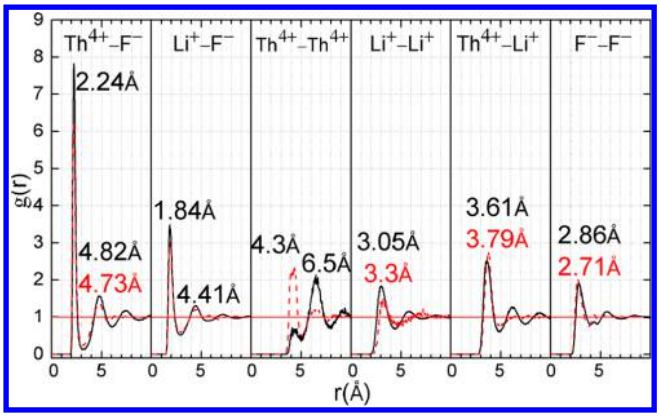

Figure 1. Radial distribution functions $g(r)$ in LiF−ThF_4 systems at 1200 K for two mole fractions (black solid line and upper numerical peak values in black: x_{ThF_4} = 0.12 (~$ThLi_7F_{11}$); red dashed line and lower numerical peak values in red: x_{ThF_4} = 0.67 (~Th_2LiF_9)).

Table 2. Counterionic (M^{q+}−F^-) Distances r in Molten Salts (MS), Sums of Ionic Radii (ΣR_I) for the Respective Coordination Numbers (CN), and Differences Δ[a]

MS	M^{q+}	CN	r	ΣR_I	Δ
LiF−ThF_4	Th^{4+}	8	2.24	2.36	0.12
LiF−YF_3	Y^{3+}	8	2.24	2.33	0.09
LiF−ZrF_4	Zr^{4+}	7	2.02	2.09	0.07
LiF	Li^{1+}	5	1.84	1.98	0.14

[a]All distances are in Å; R_{F^-}(CN = 4) = 1.17 Å; R_{Li^+}(CN = 5) = 0.82 Å is interpolated.

the counterionic distances r derived from the RDFs at 1200 K correlate well with Shannon's ionic crystal radii[40] sums at room temperature (for the respective coordination numbers, see below), but the latter are 0.1 ± 0.03 Å larger (±0.03 Å also corresponds to the reliability of the ionic radii). This unexpected sign of the discrepancy is consistent with the fact that, upon melting, the first-neighbor distance of the alkali halides decreases, while the overall volume significantly increases.[41]

The first peak for Th^{4+}−F^- is very sharp and is followed by a deep minimum, which is typical for comparatively stable, partially covalently bonded clusters with a relatively well-defined first solvation shell. Correspondingly, the RDF of Th^{4+}−F^- hardly varies with temperature. In contrast, the first peak for Li^+−F^- is broader, and the first minimum is less pronounced, indicative of a more flexible ion cluster that allows exchange of the F^- counterions more frequently. All RDFs (F^-−F^-, M^{q+}−F^-, M^{q+}−M^{q+}) show only slight variations with the ion concentrations, except the Th^{4+}−Th^{4+} one. For a high concentration of thorium (x_{ThF_4} = 0.67) there appears a pronounced Th^{4+}−Th^{4+} peak at 4.3 Å. The separation is somewhat smaller than twice the Th^{4+}−F^- bond distance and indicates a significant amount of pairs of thorium cations, bonded by nonlinear bridging fluoride anions. Such a medium-range network-like structural feature has been detected also in other molten fluorides and has an important impact on the transport properties.[8]

The differences of distance mentioned above point in the same direction. In ionic crystals, there is equal bonding in opposite directions between the counterions. However, upon melting the extended structure breaks down and expands, but

dx.doi.org/10.1021/jp509425p | J. Phys. Chem. B 2014, 118, 13954−13962

the local structure here becomes stronger. This difference is reminiscent of the overall short bond distances in aromatic rings, for which upon breaking the resonance structure the rings expand, but the formed local double bonds become shorter.

3.2. Coordination Numbers. The immediate environment of an ion is characterized by its coordination number (CN). Th^{4+} is known to be the softest tetravalent ion stable in aqueous solution.[42] Its solvation structure has often been studied experimentally and theoretically.[42−54] MD simulations by Vallet et al.[43] yielded well-structured first hydration shells of eight or nine water molecules with a mean Th−O distance of 2.45 Å. Similarly, thorium is 8-coordinate in the ThF_4 crystal.[55]

The thermal stability of the ionic complexes in the melt can be revealed by the temperature dependence of their CNs. Recently Salanne et al. reported the CNs in various melts.[17,20] We have investigated the influence of the temperature T on $[MF_n]$ species at x_{ThF_4} = 0.50. The first solvation shells of the Th^{4+} and Li^+ cations were defined by distance cutoffs at the minima in the RDFs, that is, 3.2 and 2.9 Å, respectively. For thorium (Figure 2a), three dominant complexes are found to

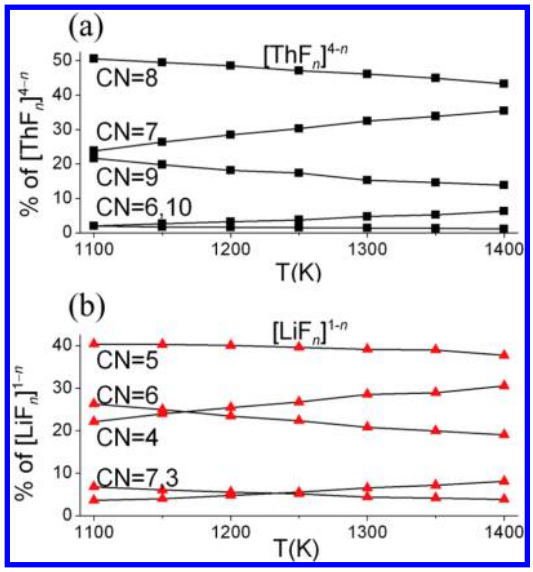

Figure 2. Temperature variation (T in K) of the percentages of fluoro complexes with coordination number CN = n in LiF−ThF_4 MS (x_{ThF_4} = 0.50): (a) Th^{4+}-centered complexes; (b) Li^+-centered complexes. (Statistical accuracy < ± 3%. Similar trends are found for other mole fractions.)

coexist in the melt: $[ThF_7]^{3-}$, $[ThF_8]^{4-}$, and $[ThF_9]^{5-}$, with the 8-fold coordinated $[ThF_8]^{4-}$ complex always being the predominant one. For lithium (Figure 2b), the 5-fold coordinated complexes are predominant besides CN = 4 and 6. As expected, for both the Th and the Li fluorides, the amount of the lower CN complexes increases with the temperature, while the amount of the higher CN complexes decreases, resulting in a slight decrease of the average CN for higher T.

The variations of the CN-percentages with the mole fractions are displayed in Figure 3. They are slightly nonlinear. The 8-fold coordinated Th complexes (Figure 3a) and the 5-fold coordinated Li complexes (Figure 3b) are predominant at all compositions. The averaged CNs (Figure 3c) vary only slightly, except for $[LiF_n]$ where n is near 5.0. But this value decreases down to less than 4.5 at lowest x_{ThF_4}. We find no evidence of any CN extrema, in particular near x-values corresponding to

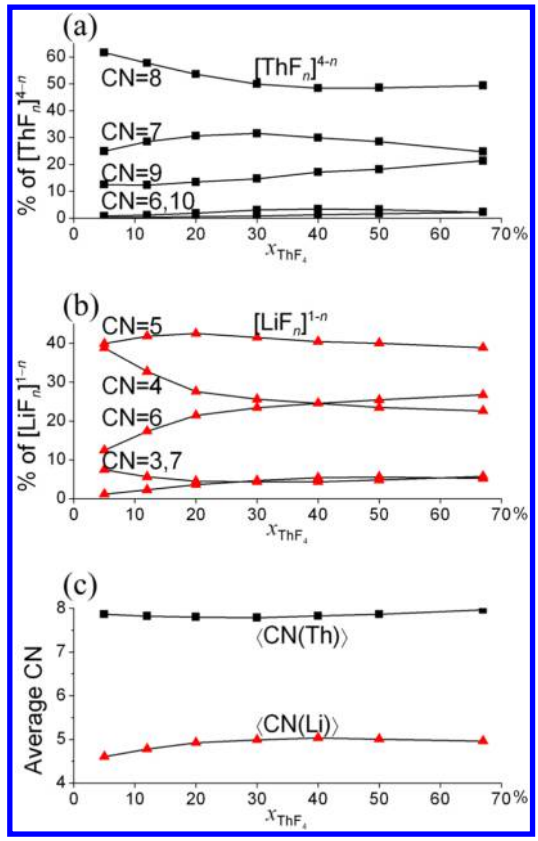

Figure 3. LiF−ThF_4 molten salts with different x_{ThF_4} at 1200 K: (a) percentages of $[ThF_n]^{4-n}$ complexes with coordination number CN = n; (b) percentages of $[LiF_n]^{1-n}$ complexes; (c) average CN of Th^{4+}- and Li^+-centered complexes (statistical accuracy < ± 2%).

the solid compounds $[Li_3ThF_7]$ (x_{ThF_4} = 0.25) and $[Li_7Th_6F_{31}]$ (x_{ThF_4} = 0.46),[30] while Pauvert et al.[18] had found such extrema for the LiF−ZrF_4 system at the composition of $[ZrF_6]Li_2$.

3.3. ^{19}F NMR Chemical Shifts. The ^{19}F NMR spectra for LiF−ThF_4 systems at different x_{ThF_4} were reported by Bessada et al.[10] At the high temperature of the MS, the fluoride ion exchange is fast enough so that only one sharp peak is observed, corresponding to the weighted average of environments.[1] The fluoride anions in LiF−ThF_4 MS can be categorized into three kinds: (i) F^- with neighboring Li^+ and F^- but no Th^{4+} in the first solvation shell; (ii) F^- with just one Th^{4+} in its first solvation shell; (iii) F^- with two adjacent Th^{4+} ions (i.e., in bent Th^{4+}−F^-−Th^{4+} bridges). The mean chemical shift in the LiF−ThF_4 melt can then be expressed as $\delta = \Sigma_{i=1-3}\, \omega_i\delta_i$, where ω_i is the fraction of a particular kind of F^- and δ_i is the corresponding chemical shift. For fluorine atoms of type (i), the value of the pure LiF melt may be assumed for the ^{19}F chemical shift (δ_1 = −200 ppm).[10] For fluorine atoms of type (iii), one may assume the value of the pure ThF_4 melt (δ_3 = +115 ppm).[10] The fractions ω_i of the three kinds of F^- ions for different compositions x_{ThF_4} are obtained from the MD simulations. Combining the calculated ω_i values and the measured shifts δ, and the assumed δ_1 and δ_3 values, an optimized fit (Figure 4) yields δ_2 = −30 ppm. The (Th−)F(−Li) shift δ_2 is about the mean value of the (Li−)F(−Li) and (Th−)F(−Th) shifts δ_1 and δ_3. The agreement between experiment and theoretical fit is quite satisfactory. The fit-curve is convex, as was also found

dx.doi.org/10.1021/jp509425p | J. Phys. Chem. B 2014, 118, 13954−13962

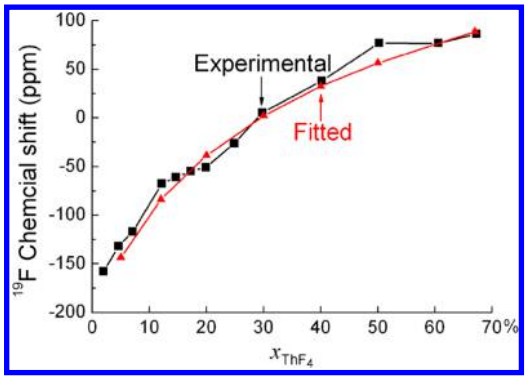

Figure 4. Experimental and semitheoretical values (with fitted δ_2 parameter) of ^{19}F chemical shifts for LiF−ThF_4 molten salts vs the mole fraction x_{ThF_4} at 1200 K.

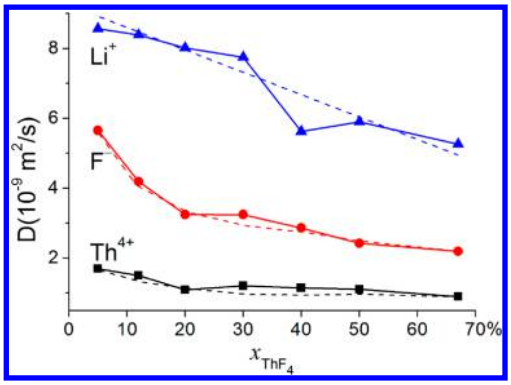

Figure 5. Diffusion coefficients of Li^+ (top line), F^- (middle line), and Th^{4+} (bottom line), in LiF−ThF_4 melts at 1200 K vs x_{ThF_4}. (The dashed curves are drawn to guide the eye.).

experimentally for alkali rare-earth AF−LnF_3 mixtures (A = Li, Na, K, Rb; Ln = La, Y, Ce, Lu),[56,57] where the fluoride ions also rapidly exchange between the three environments.[1]

3.4. Macroscopic Properties of LiF−ThF_4 Melts.

Densities. The calculated densities ρ_{MD} of the MS at T = 1100 to 1400 K and x_{ThF_4} = 0.5 were fitted to a linear relation and compared to the experimentally deduced fit of Meaker et al. (ρ_{Exp})[58] and to the theoretical fit of Salanne et al. (ρ_{Sal}):[33]

$$\rho_{MD}/\mathrm{g{\cdot}cm^{-3}} = 6.417 - 1.160T/1000\ \mathrm{K} \quad (1.MD)$$

$$\rho_{Exp}/\mathrm{g{\cdot}cm^{-3}} = 6.677 - 1.165T/1000\ \mathrm{K} \quad (1.Exp)$$

$$\rho_{Sal}/\mathrm{g{\cdot}cm^{-3}} = 7.058 - 1.536T/1000\ \mathrm{K} \pm 1.5\% \quad (1.Sal)$$

Our values are small by about 5%, while Salanne's values deviate by only up to 2.5% in the mentioned temperature range from the experimental data of unknown accuracy.

Transport Coefficients. The diffusion coefficients D of Th^{4+}, Li^+, and F^- were obtained for x = 0.50 and $T \approx$ 1250 K from Einstein's diffusion relation, and were fitted by Arrhenius-type relations (the values from Dewan et al. for x = 0.22 are listed in parentheses):

$$\ln[D_{Th}/\mathrm{m^2s^{-1}}] = -16.163 - 5307\ \mathrm{K}/T \quad (-15.694)(-5786\mathrm{K}) \quad (2.Th)$$

$$\ln[D_{Li}/\mathrm{m^2s^{-1}}] = -15.237 - 4452\ \mathrm{K}/T \quad (-15.362)(-4052\mathrm{K}) \quad (2.Li)$$

$$\ln[D_{F}/\mathrm{m^2s^{-1}}] = -16.403 - 4028\mathrm{K}/T \quad (-15.674)(-4594\mathrm{K}) \quad (2.F)$$

Dewan's diffusion coefficients for the lower Th concentration (x = 0.22) are larger than ours (x = 0.5) by 7% for Th, and by around 25% for Li and F. The variation of D vs x_{ThF_4} at 1200 K is presented in Figure 5. Indeed, the diffusion becomes slower upon increase of the Th concentration, in particular for Li and F, indicating structure-formation in the melt through the creation of $ThF_{8\pm1}$ complexes. Anyway, the order of the diffusion coefficients is found to be $Li^+ > F^- > Th^{4+}$ with ratios around 1:0.5:0.2. The corresponding activation energies for the diffusion hopping in the $ThLiF_5$ ($ThLi_{3.5}F_{7.5}$) melts are 44.1 (41.8) kJ/mol for Th, 37.0 (33.7) kJ/mol for Li, and 33.5 (38.2) kJ/mol for F, respectively.

The Einstein relation was also applied in the MD simulations to determine the electrical conductivity, σ_{MD}.[59] Neglecting the ion correlations, the conductivity was also estimated by the Nernst−Einstein approximation, σ_{NE}.[59] Again, the values can be fitted by Arrhenius-type equations, which can be expressed in linear or exponential Arrhenius form (see Appendix 1). They are compared with the theoretical values σ_{De} of Dewan et al.,[19] as well as with the experimental values, σ_{Exp},[58] here for two different concentrations of Th (x = 0.50 and 0.22; $\theta = T/1000$ K):

x_{ThF_4} = 0.50:

$$\sigma_{MD}{\cdot}\Omega\ \mathrm{cm} = -2.816 + 4.060\theta$$
$$\text{or } \ln[\sigma_{MD}{\cdot}\Omega\ \mathrm{cm}] = 3.090 - 2.844/\theta$$
$$(\sigma_{MD}{}^{1200K} = 2.1\ \mathrm{S/cm}) \quad (3.MD)$$

$$\sigma_{NE}{\cdot}\Omega\ \mathrm{cm} = -7.915 + 11.02\theta$$
$$\text{or } \ln[\sigma_{NE}{\cdot}\Omega\ \mathrm{cm}] = 4.160 - 2.989/\theta$$
$$(\sigma_{NE}{}^{1200K} = 5.3\ \mathrm{S/cm}) \quad (3.NE)$$

$$\sigma_{Exp}{\cdot}\Omega\ \mathrm{cm} = -2.446 + 4.186\theta$$
$$\text{or } \ln[\sigma_{Exp}{\cdot}\Omega\ \mathrm{cm}] = 2.896 - 2.339/\theta$$
$$(\sigma_{Exp}{}^{1200K} = 2.6\ \mathrm{S/cm}) \quad (3.Exp)$$

x_{ThF_4} = 0.22:

$$\sigma_{De}\Omega\ \mathrm{cm} = -4.173 + 7.411{\cdot}\theta$$
$$\text{or } \ln[\sigma_{De}{\cdot}\Omega\ \mathrm{cm}] = 3.436 - 2.261/\theta$$
$$(\sigma_{De}{}^{1200K} = 4.7\ \mathrm{S/cm}) \quad (4.De)$$

$$\sigma_{Exp}{\cdot}\Omega\ \mathrm{cm} = -4.421 + 7.580\theta$$
$$\text{or } \ln[\sigma_{Exp}{\cdot}\Omega\ \mathrm{cm}] = 3.488 - 2.335/\theta$$
$$(\sigma_{Exp}{}^{1200K} = 4.7\ \mathrm{S/cm}) \quad (4.Exp)$$

The directly calculated electrical conductivity (3.MD) is closer to the experimentally derived one (3.Exp) than the Nernst−Einstein approximation (3.NE), which is known for its tendency toward overestimation.[60] In the pertinent temperature ranges, the values of eqs 3.MD, 3.Exp for x = 0.50 are

dx.doi.org/10.1021/jp509425p | J. Phys. Chem. B 2014, 118, 13954−13962

about one-half of those of eqs (4) for $x = 0.22$. The calculated electrical conductivities and some experimental results[58] for different x_{ThF_4} are displayed in Figure 6, which also shows that the σ increases upon decrease of x value. On the whole, our calculated values are in agreement with the experimental results.[61]

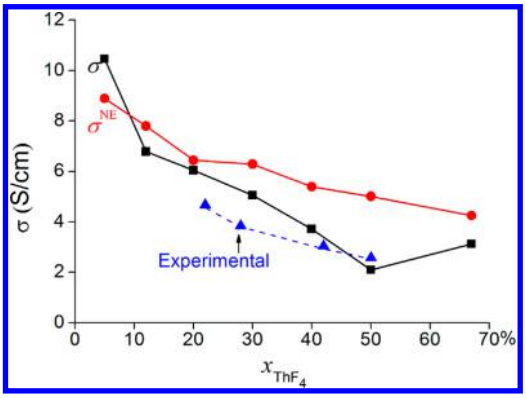

Figure 6. Electrical conductivity of LiF−ThF_4 molten salt as a function of x_{ThF_4} at 1200 K.

3.5. Electronic Structure of the $[ThF_8]^{4-}$ Complexes.

Th^{4+} has a larger ionic radius than most transition metals and can possess higher coordination numbers than six.[62] Indeed our MD simulations show that the CNs of Th^{4+} lie around 7 to 9. From selected snapshots of the MD trajectories of a diluted LiF−ThF_4 melt, we have cut out the local arrangements of ions around a single Th^{4+} ion. In a typical cluster of $[ThF_8]^{4-}(Li_{N+4}F_N)^{4+}$ with N around 20, the central $[ThF_8]^{4-}$ complex is surrounded in a second and third solvation shell by a total of N +4 Li^+ and N F^- ions (Figure 7). An electronic valence orbital energy band structure, obtained by quantum chemical calculations with the ADF program at the density-functional and relativistic spin-averaged level, is shown in Figure 8.

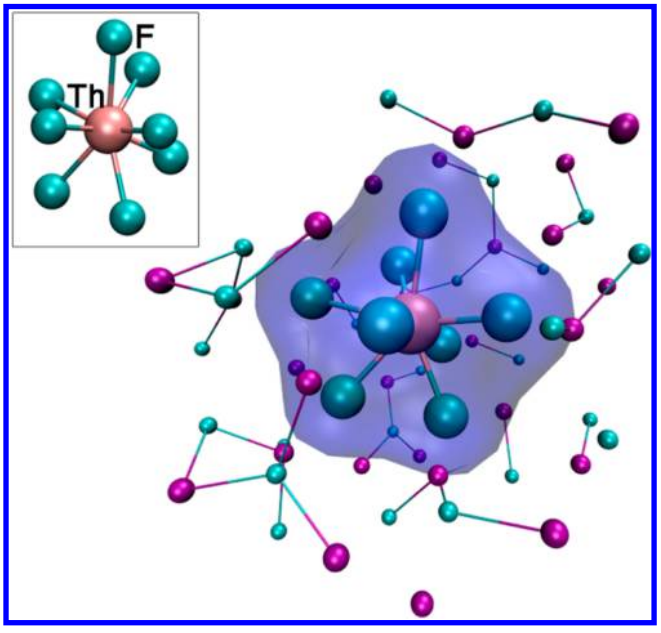

Figure 7. A $[ThF_8]Li_{28}F_{24}$ cluster. Insert: The central $[ThF_8]^{4-}$ cluster ion.

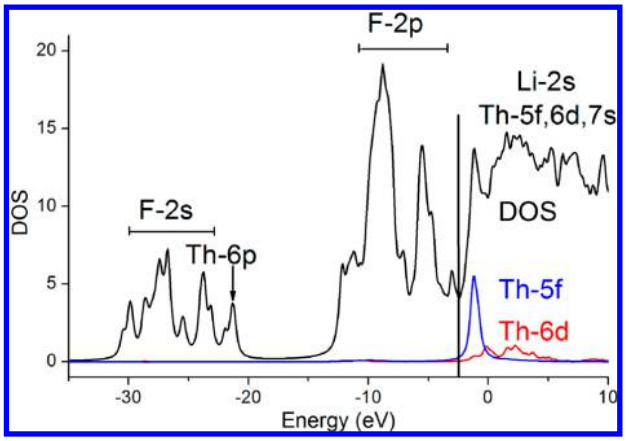

Figure 8. DFT-PBE total density of electronic valence states (DOS) of a $[ThF_8](Li_{23}F_{19})$ cluster, of occupied F-2s, F-2p, and Th-6p character, and of virtual Th-5f, Th-6d, and Th-7s character. The Th-5f (blue) and Th-6d (red) partial DOS are also shown. The vertical line indicates the Fermi (HOMO) energy.

The F-2s type orbitals above −30 eV are filled and may be counted as atomic core orbitals, their energies here being modulated a bit by the electric ion field varying over the cluster. The Th-6p shell around −22 eV is not completely filled (see Figure 8). As usual, the early actinide atoms, when coordinated to electronegative ligands, exhibit spin−orbit split An-6p holes. That is, the outer radon $6p^6$ shell is already so weakly bound and so soft that it no longer behaves as a real inert "noble" gas core−shell. Beyond −12 eV there begins the F-2p type band with some Th-6p, Th-6d, and Th-5f admixture. Above the Fermi level, there is a rather sharp virtual band of highly localized Th-5f character, then come broad conduction bands of Th-6d and Th-7s character.

Averaged atomic orbital (AO) populations of the $ThLi_{n+4}F_{n+8}$ model cluster are displayed in Table 3. The charges indicate highly ionic atoms F^{1-}, Li^{1+}, and Th^{4+}. The hard F^- ions are hardly polarized, with negligible F-3d4f population, and they donate a little F-2s2p charge into the 2s2p shell of Li^+, and a little more than four times that into the 5f6d shell of Th^{4+}. Simultaneously, the F^- ligands squeeze more than 0.4 electrons out of the soft [Rn-$6s^26p^6$] semicore−shell of Th, which overlaps a bit with the F-$2s^22p^6$ shells. The calculated bond order indices based on different schemes are displayed in Table 4. They all indicate more covalent character for the Th−F than for the Li−F interactions.

3.6. Structure and Dynamics of $[ThF_8]^{4-}$.

Salanne et al. had recently reported the fluorine-ligand escape ("cage-out") times[66] from the first coordination shell of Zr^{4+} in AF−ZrF_4 melts (A = Li, Na and K),[17] and from Y^{3+} in LiF−YF_3 melts.[20] From the temperature dependence, the activation energies of the dissociation $[MF_n] \rightarrow [MF_{n-1}] + F$ in the MS were determined, which are relevant for the transport processes. Although Zr and Y have similar CN of $n \approx 8$, the interaction of Y^{3+}−F^- seems weaker than that of Zr^{4+}−F^-, likely due to the different electrostatic interactions.[20] We have investigated the dissociative behavior of the $[ThF_n]$ clusters in the LiF−ThF_4 melts, with the first coordination shell being defined as before by r(Th−F) ≤ 3.2 Å. We have chosen T = 1200 K and x_{ThF_4} = 0.35, which allows for comparison with previous works. The F^- cage-out time τ is defined as the time needed for a statistical fraction of $1/e$ (e = 2.718···) of the F-ions having left $[ThF_n]$ (Figure 9). These times in LiF−MF_n melts are 0.7 ps for M =

dx.doi.org/10.1021/jp509425p | J. Phys. Chem. B 2014, 118, 13954−13962

Table 3. Average Mulliken Populations of Several $[ThLi_{N+4}F_{N+8}]^0$ Clusters ($N \approx 20$)

atom	charge	AO populations[a]			
Th	+3.4 ± 1/2	Th-6s^2	Th-6p^6	Th-6d^0	Th-5f^0
		−0.4 ± 0.2	−0.3 ± 0.1	+0.5 ± 0.2	+0.8 ± 0.1
$Li_{(solvent)}$ (mean)	+0.66	Li-2s^0	Li-2p^0	Li-3d^0	Li-4f^0
		+0.08	+0.18	+0.06	+0.01
$F_{(ThF8)}$ (mean)	−0.74	F-2s^2	F-2p^6	F-3d^0	F-4f^0
		+0.06	−0.31	+0.01	+0.00
$F_{(solvent)}$ (mean)	−0.66	F-2s^2	F-2p^6	F-3d^0	F-4f^0
		−0.04	−0.39	+0.00	+0.00

[a]Negative values mean depopulation of the otherwise fully occupied shell given as reference in the headline.

Table 4. Average Bond Orders (BO)[a] in $[ThLi_{N+4}F_{N+8}]^0$ Clusters ($N \approx 20$)

	BO_M	$BO_{G\text{-}J}$	$BO_{N\text{-}M2}$
Th−F	0.1−0.2	0.45−0.5	1.5 ± 0.1
Li−F	∼0.25	∼0.12	∼0.8

[a]BO_M: Mayer bond order;[63] $BO_{G\text{-}J}$: Gophinatan−Jug bond order;[64] $BO_{N\text{-}M2}$: Nalewajski-Mrozek bond order (includes covalent and ionic contributions).[65]

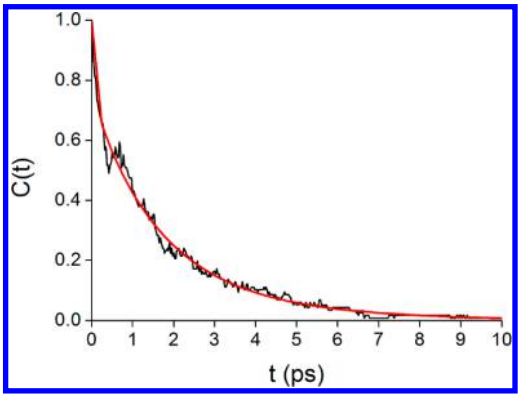

Figure 9. Probability $C(t)$ for an F-ligand to leave the first coordination shell of $[ThF_n]^{4-n}$ complex ions in an LiF−ThF_4 melt (x_{ThF_4} = 0.35, T = 1200 K) within time t (in ps). The red line is the fitted exponential decay curve.

Y,[20] 1.0 ± 0.2(1σ) ps for M = Th (this work), and 3.1 ps for M = Zr.[17] We note that *at room temperature* the lifetime of a water ligand in the equatorial plane of the uranyl cation in water solution, $[UO_2]^{2+}\cdot(H_2O)_n$, is nearly 3 orders of magnitude longer (775 ps).

According to transition state theory,[67,68] the rate at which F^- ions escape from the first Th^{4+} coordination shell is determined by the height of the corresponding potential energy barrier. The average effective potential curve $V(r)$ for the $Th^{4+}F^-_{n+1} \rightarrow Th^{4+}F^-_n + F^-$ dissociation can be estimated from the radial distribution functions $g_{ij}(r)$ discussed above:

$$V(r) = -k_B T \ln g_{ij}(r) \quad (5)$$

This potential is plotted in Figure 10 and shows a deep minimum followed by a local maximum. The energy barrier for the Th^{4+}−F^- dissociation obtained from $V(r)$ is 3.5k_BT (i.e., 35 kJ/mol at 1200 K), which is smaller than the value for the LiF−ZrF_4 melt (4.5k_BT) and larger than the value for the LiF−YF_3 melt (3.0k_BT). The calculated energy barriers for M−F dissociation in LiF−MF_n melts are consistent with the trend of the escape times mentioned above. The activation energies of the F_n-shell decay of $[ThF_n]$ and of the F diffusion (34.4 and 33.5 kJ/mol) are remarkably similar. The results support suggestions of Salanne et al. that the radial distribution function $g(r)$ is a better indicator of complex dynamics than the coordination number,[20] which is the integral over the first wiggle of $g(r)$. The $[MF_n]$-complex decay times in the LiF melts vary with the activation energies and temperatures as

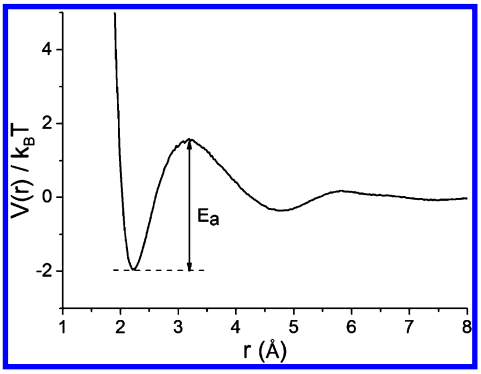

Figure 10. Mean effective potential energy $V(r)$ (in k_BT) for Th^{4+}−F^- dissociation in an LiF−ThF_4 melt (x_{ThF_4} = 0.35, T = 1200 K).

$$\tau = 0.03(\text{ps})\ \exp(E_a/k_BT) \quad (6)$$

where E_a can be obtained from $g(r)$ via eq 5. To verify the applicability of eq 6, we have performed MD simulations for x_{ThF_4} = 0.35 at two other different temperatures (T = 1000 and 1400 K). The decay times calculated from the radial distribution function $g(r)$ (eq 6) are 1.2 and 0.9 ps, respectively, whereas the values calculated from the cage-out function $C(t)$ are 1.5 and 0.6 ps, which roughly agree with each other.

In a dynamic process, the metal complex ions $[MF_n]^{q-}$ rearrange in the melt by adding and losing fluorine ligands in the coordination or solvation shells. We have determined the reaction rates for the various cage-out and cage-in processes at T = 1200 K and the results are listed in Table 5. These rates determine the individual mean lifetimes $\tau_n = 1/(k_{n\rightarrow n+1} + k_{n\rightarrow n-1})$ of the $[ThF_n]$ complex species and their relative concentrations. The formulas used for evaluating the lifetimes are presented in Appendix 2. The respective average cage-out lifetime is 0.9 ps, to be compared to the above-mentioned value of 1.0 ± 0.2 ps. For increasing size n of the first Th coordination shell of $[ThF_n]^{q-}$, the dissociation rate $k_{n\rightarrow n-1}$

dx.doi.org/10.1021/jp509425p | J. Phys. Chem. B 2014, 118, 13954−13962

Table 5. Cage-out and Cage-in Reaction Rates of $[ThF_n]$ Clusters in LiF−ThF_4 Molten Salt[a]

n[b]	6	7	8	9	10
c_n	2.5%	30%	50%	16%	1%
cage-out	5←6	6←7	7←8	8←9	9←10
$k_{n\to n-1}$	≪0.1	0.93 ± 0.15	3.5 ± 0.2	9.2 ± 1.1	21. ± 5.
cage-in	6→7	7→8	8→9	9→10	10→11
$k_{n\to n+1}$	11. ± 2.	6.1 ± 0.6	2.9 ± 0.3	1.4 ± 0.3	<0.1

[a]For x_{ThF_4} = 0.35, T = 1200 K, time-step =2.5 fs. [b]n is the number of F ligands, c_n is mole fraction of $[ThF_n]$ in % (±1/2%), k is rate constant in ps^{-1} (±1σ).

increases steadily, while the association rate $k_{n\to n+1}$ steadily decreases. The crossover occurs just below that n value for which the maximum concentration is reached.

4. SUMMARY AND CONCLUSIONS

We have investigated the local structure around Th^{4+} in LiF−ThF_4 melts by MD simulations. We find that the coordination number of $[Th^{4+}F^-_n]^{4-n}$ is 8 ± 1 under the simulation conditions. Although the average coordination number hardly varies with the composition of the melt, it changes with the temperature, in accordance with the results of other molten salts.[17,20] Our results reveal that there coexist mainly three different thorium complexes $[ThF_7]^{3-}$, $[ThF_8]^{4-}$, and $[ThF_9]^{5-}$, at concentration ratios near 2:3:1 around T = 1200 K. The individual $[MF_n]$ clusters in the hot melt are more compact than in the low-temperature solid phase, while the overall melt is expanded. The F^- anions occur in three different environments, either coordinated to Li^+ only, or also to one Th^{4+}, or bridging two Th^{4+} cations. The three types of fluoride anions exhibit different NMR shifts of −200 ppm, −30 ppm, and +115 ppm, respectively. The atomic species in the LiF−ThF_4 melts behave as nearly ideal ions, only the $[ThF_{8\pm1}]^{-4\pm1}$ complex clusters exhibit partially covalent $Th^{4+} \leftarrow F^-$ dative coordination bonds from F-2p to Th-5f6d.

The lifetime τ of the first solvation or complex-coordination shell of Th^{4+}, corresponding to a $1/e$ probability of one F atom entering or leaving the ThF_n complex, has been determined through the time-variation of the coordination number. As noted by Salanne,[20] the stability of MF_n complexes in molten salts is not directly related to the coordination number n but to the decay activation energy. The latter is empirically related to the Th^{4+}−F^- radial pair-distribution function $g_{ThF}(r)$, which is easily available from MD simulations. Our results show that a basic understanding of the physical and chemical properties of actinides in molten salts can be obtained through molecular dynamics simulations combined with quantum chemical bonding analyses and experimental spectroscopic analyses. Further computational study of the MD simulation results using a network analysis approach[69] will be interesting for understanding the patterns and organization as well as various physical properties and chemical reactivity of actinide molten salt systems.

APPENDIX

1. Linear Approximation of the Arrhenius Curve

In a finite temperature range around T_1, the Arrhenius relation $y = a\exp(-b/T)$ may be approximated by a linear relation $y = -c + dT$. Assuming the value and temperature derivative being equal at T_1, one obtains the relations

$$y_1 = a\exp(-b/T_1) = (dT_1 - c) \tag{A1a}$$

and

$$(dy/dT)_1 = d = b(dT_1 - c)/T_1^2 \tag{A1b}$$

which yields the linear parameters c,d, in terms of the Arrhenius parameters a,b, and vice versa the Arrhenius parameters in terms of its linear approximation parameters, respectively:

$$a = (dT_1 - c)\exp(dT_1/(dT_1 - c)), \quad b = dT_1^2/(dT_1 - c) \tag{A2a}$$

$$c = a\exp(-b/T_1)(b/T_1 - 1), \quad d = a\exp(-b/T_1)b/T_1^2 \tag{A2b}$$

2. On the Lifetime of $[MF_n]$ Complexes

The dominant Th species in the LiF melt is $[ThF_8]^{4-}$. Its coordination shell can rearrange by losing or adding an F ligand, yielding $[ThF_7]^{3-}$ or $[ThF_9]^{5-}$. Let the relative concentrations of the $[ThF_n]^{(n-4)-}$ species be c_n, with $\sum_n c_n = 1$, and the rate constants be denoted by $k_{n\to n-1}$ and $k_{n\to n+1}$. Then, at equilibrium

$$c_n k_{n\to n+1} = c_{n+1}k_{n+1\to n} \tag{A3}$$

which yields the equilibrium concentrations. The lifetime of complex $[ThF_n]$ is thus

$$\tau_n = 1/(k_{n\to n+1} + k_{n\to n-1}) \tag{A4}$$

ASSOCIATED CONTENT

Supporting Information

Polarizable ion model potential description and corresponding parameters. This material is available free of charge via the Internet at http://pubs.acs.org.

AUTHOR INFORMATION

Corresponding Author

* E-mail: junli@tsinghua.edu.cn. Tel./Fax: +86-10-62797472.

Notes

The authors declare no competing financial interest.

[§]Mailing Address: W.H.E.S.: Physical and Theoretical Chemistry Laboratory, Faculty of Science and Engineering, University of Siegen, 57068 Siegen, Germany (E-mail: eugen.schwarz@uni-siegen.de).

ACKNOWLEDGMENTS

The authors would like to thank Dr. E. Bylaska, Dr. D. Perez, and Prof. M. Salanne for helpful discussions. This work was financially supported by the National Key Basic Research Special Foundations (No.2013CB834603) and the National Natural Science Foundation of China (Nos. 21433005, 91026003, 11079006). The calculations were performed at Tsinghua National Laboratory for Information Science and Technology. A portion of the calculations was performed using

EMSL, a national scientific user facility sponsored by the U.S. Department of Energy's Office of Biological and Environmental Research and located at the Pacific Northwest National Laboratory of the USA.

REFERENCES

(1) Sarou-Kanian, V.; Rollet, A. L.; Salanne, M.; Simon, C.; Bessada, C.; Madden, P. A. Diffusion Coefficients and Local Structure in Basic Molten Fluorides: In Situ NMR Measurements and Molecular Dynamics Simulations. *Phys. Chem. Chem. Phys.* **2009**, *11*, 11501−11506.

(2) Kimura, I. Review of Cooperative Research on Thorium Fuel Cycle as a Promising Energy Source in the Next Century. *Prog. Nucl. Energy* **1995**, *29*, 445−452.

(3) Gat, U.; Engel, J. R. Non-proliferation Attributes of Molten Salt Reactors. *Nucl. Eng. Des.* **2000**, *201*, 327−334.

(4) Oh, S. K.; Chung, K. AMBIDEXTER Nuclear Energy Complex: A Practicable Approach for Rekindling Nuclear Energy Application. *Nucl. Eng. Des.* **2001**, *207*, 11−19.

(5) Nuttin, A.; Heuer, D.; Billebaud, A.; Brissot, R.; Le Brun, C.; Liatard, E.; Loiseaux, J. M.; Mathieu, L.; Meplan, O.; Merle-Lucotte, E.; et al. Potential of Thorium Molten Salt Reactors: Detailed Calculations and Concept Evolution with a View to Large Scale Energy Production. *Prog. Nucl. Energy* **2005**, *46*, 77−99.

(6) Mathieu, L.; Heuer, D.; Brissot, R.; Garzenne, C.; Le Brun, C.; Lecarpentier, D.; Liatard, E.; Loiseaux, J. M.; Meplan, O.; Merle-Lucotte, E.; et al. The Thorium Molten Salt Reactor: Moving on from the MSBR. *Prog. Nucl. Energy* **2006**, *48*, 664−679.

(7) Heaton, R. J.; Brookes, R.; Madden, P. A.; Salanne, M.; Simon, C.; Turq, P. A First-Principles Description of Liquid BeF_2 and Its Mixtures with LiF: 1. Potential Development and Pure BeF_2. *J. Phys. Chem. B* **2006**, *110*, 11454−11460.

(8) Salanne, M.; Simon, C.; Turq, P.; Heaton, R. J.; Madden, P. A. A First-Principles Description of Liquid BeF_2 and its Mixtures with LiF: 2. Network Formation in LiF−BeF_2. *J. Phys. Chem. B* **2006**, *110*, 11461−11467.

(9) Akdeniz, Z.; Madden, P. A. Raman Spectra of Ionic Liquids: A Simulation Study of AlF_3 and its Mixtures with NaF. *J. Phys. Chem. B* **2006**, *110*, 6683−6691.

(10) Bessada, C.; Rakhmatullin, A.; Rollet, A. L.; Zanghi, D. Lanthanide and Actinide Speciation in Molten Fluorides: A Structural Approach by NMR and EXAFS Spectroscopies. *J. Nucl. Mater.* **2007**, *360*, 43−48.

(11) van der Meer, J.; Konings, R. Thermal and Physical Properties of Molten Fluorides for Nuclear Applications. *J. Nucl. Mater.* **2007**, *360*, 16−24.

(12) Rollet, A. L.; Godier, S.; Bessada, C. High Temperature NMR Study of the Local Structure of Molten LaF_3−AF (A = Li, Na, K and Rb) Mixtures. *Phys. Chem. Chem. Phys.* **2008**, *10*, 3222−3228.

(13) Salanne, M.; Simon, C.; Turq, P.; Madden, P. A. Heat-Transport Properties of Molten Fluorides: Determination from First-Principles. *J. Fluorine Chem.* **2009**, *130*, 38−44.

(14) Numakura, M.; Sato, N.; Bessada, C.; Okamoto, Y.; Akatsuka, H.; Nezu, A.; Shimohara, Y.; Tajima, K.; Kawano, H.; Nakahagi, T.; et al. Structural Investigation of Thorium in Molten Lithium-Calcium Fluoride Mixtures for Salt Treatment Process in Molten Salt Reactor. *Prog. Nucl. Energy* **2011**, *53*, 994−998.

(15) Rollet, A. L.; Salanne, M.; Groult, H. Structural Effects on the Electrical Conductivity of Molten Fluorides: Comparison between LiF−YF_3 and LiF−NaF−ZrF_4. *J. Fluorine Chem.* **2012**, *134*, 44−48.

(16) Salanne, M.; Simon, C.; Groult, H.; Lantelme, F.; Goto, T.; Barhoun, A. Transport in Molten LiF−NaF−ZrF_4 Mixtures: A Combined Computational and Experimental Approach. *J. Fluorine Chem.* **2009**, *130*, 61−66.

(17) Pauvert, O.; Salanne, M.; Zanghi, D.; Simon, C.; Reguer, S.; Thiaudiere, D.; Okamoto, Y.; Matsuura, H.; Bessada, C. Ion Specific Effects On the Structure of Molten AF−ZrF_4 Systems (A^+ = Li^+, Na^+, and K^+). *J. Phys. Chem. B* **2011**, *115*, 9160−9167.

(18) Pauvert, O.; Zanghi, D.; Salanne, M.; Simon, C.; Rakhmatullin, A.; Matsuura, H.; Okamoto, Y.; Vivet, F.; Bessada, C. In Situ Experimental Evidence for a Nonmonotonous Structural Evolution with Composition in the Molten LiF−ZrF_4 System. *J. Phys. Chem. B* **2010**, *114*, 6472−6479.

(19) Dewan, L. C.; Simon, C.; Madden, P. A.; Hobbs, L. W.; Salanne, M. Molecular Dynamics Simulation of the Thermodynamic and Transport Properties of the Molten Salt Fast Reactor Fuel LiF−ThF_4. *J. Nucl. Mater.* **2013**, *434*, 322−327.

(20) Levesque, M.; Sarou-Kanian, V.; Salanne, M.; Gobet, M.; Groult, H.; Bessada, C.; Madden, P. A.; Rollet, A. L. Structure and Dynamics in Yttrium-Based Molten Rare Earth Alkali Fluorides. *J. Chem. Phys.* **2013**, *138*, 184503.

(21) Beneš, O.; Konings, R. J. M. Thermodynamic Properties and Phase Diagrams of Fluoride Salts for Nuclear Applications. *J. Fluorine Chem.* **2009**, *130*, 22−29.

(22) Beneš, O.; Beilmann, M.; Konings, R. J. M. Thermodynamic Assessment of the LiF−NaF−ThF_4−UF_4 System. *J. Nucl. Mater.* **2010**, *405*, 186−198.

(23) Khokhlov, V.; Ignatiev, V.; Afonichkin, V. Evaluating Physical Properties of Molten Salt Reactor Fluoride Mixtures. *J. Fluorine Chem.* **2009**, *130*, 30−37.

(24) van der Meer, J. P. M.; Konings, R. J. M.; Oonk, H. A. J. Thermodynamic Assessment of the LiF−BeF_2−ThF_4−UF_4 System. *J. Nucl. Mater.* **2006**, *357*, 48−57.

(25) Toth, L. M.; Boyd, G. E. Raman Spectra of Thorium (IV) Fluoride Complex Ions in Fluoride Melts. *J. Phys. Chem.* **1973**, *77*, 2654−2657.

(26) Vergnes, J.; Lecarpentier, D. The AMSTER Concept (Actinides Molten Salt Transmuter). *Nucl. Eng. Des.* **2002**, *216*, 43−67.

(27) Le Brun, C. Molten Salts and Nuclear Energy Production. *J. Nucl. Mater.* **2007**, *360*, 1−5.

(28) Delpech, S.; Merle-Lucotte, E.; Heuer, D.; Allibert, M.; Ghetta, V.; Le-Brun, C.; Doligez, X.; Picard, G. Reactor Physic and Reprocessing Scheme for Innovative Molten Salt Reactor System. *J. Fluorine Chem.* **2009**, *130*, 11−17.

(29) Thoma, R. E.; Insley, H.; Landau, B. S.; Friedman, H. A.; Grimes, W. R. Phase Equilibria in the Fused Salt Systems LiF−ThF_4 and NaF−ThF_4. *J. Phys. Chem.* **1959**, *63*, 1266−1274.

(30) Capelli, E.; Beneš, O.; Beilmann, M.; Konings, R. J. M. Thermodynamic Investigation of the LiF−ThF_4 System. *J. Chem. Thermodyn.* **2013**, *58*, 110−116.

(31) Salanne, M.; Rotenberg, B.; Jahn, S.; Vuilleumier, R.; Simon, C.; Madden, P. A. Including Many-Body Effects in Models for Ionic Liquids. *Theor. Chem. Acc.* **2012**, *131*, 1143.

(32) Salanne, M.; Madden, P. A. Polarization Effects in Ionic Solids and Melts. *Mol. Phys.* **2011**, *109*, 2299−2315.

(33) Gheribi, A. E.; Corradini, D.; Dewan, L.; Chartrand, P.; Simon, C.; Madden, P. A.; Salanne, M. Prediction of the Thermophysical Properties of Molten Salt Fast Reactor Fuel from First-Principles. *Mol. Phys.* **2014**, *112*, 1305−1312.

(34) Hutter, J.; Iannuzzi, M.; Schiffmann, F.; VandeVondele, J. CP2K: Atomistic Simulations of Condensed Matter Systems. *WIREs Comput. Mol. Sci.* **2014**, *4*, 15−25.

(35) Baerends, E. J.; Ziegler, T.; Autschbach, J.; Bashford, D.; et al. ADF 2013, SCM, *Theoretical Chemistry*; Vrije Universiteit: Amsterdam, The Netherlands, 2013

(36) Perdew, J. P.; Burke, K.; Ernzerhof, M. Generalized Gradient Approximation Made Simple. *Phys. Rev. Lett.* **1996**, *77*, 3865−3868.

(37) Chang, C.; Pelissier, M.; Durand, P. Regular Two-Component Pauli-like Effective Hamiltonians in Dirac Theory. *Phys. Scr.* **1986**, *34*, 394−404.

(38) van Lenthe, E.; Baerends, E.; Snijders, J. G. Relativistic Regular Two-Component Hamiltonians. *J. Chem. Phys.* **1993**, *99*, 4597−4610.

(39) van Lenthe, E.; Baerends, E. J. Optimized Slater-Type Basis Sets for the Elements 1−118. *J. Comput. Chem.* **2003**, *24*, 1142−1156.

(40) Shannon, R. D. Revised Effective Ionic Radii and Systematic Studies of Interatomic Distances in Halides and Chalcogenides. *Acta Cryst. A* **1976**, *32*, 751−767.

(41) Revere, M.; Tosi, M. P. Structure and Dynamics of Molten Salts. *Rep. Prog. Phys.* **1986**, *49*, 1001−1081.
(42) Wilson, R. E.; Skanthakumar, S.; Burns, P. C.; Soderholm, L. Structure of the Homoleptic Thorium(IV) Aqua Ion $[Th(H_2O)_{10}]Br_4$. *Angew. Chem., Int. Ed.* **2007**, *46*, 8043−8045.
(43) Real, F.; Trumm, M.; Vallet, V.; Schimmelpfennig, B.; Masella, M.; Flament, J. P. Quantum Chemical and Molecular Dynamics Study of the Coordination of Th(IV) in Aqueous Solvent. *J. Phys. Chem. B* **2010**, *114*, 15913−15924.
(44) Yang, T. X.; Tsushima, S.; Suzuki, A. Chloride Concentration and Temperature Effects on the Hydration of Th(IV) Ion: A Molecular Dynamics Simulation. *Chem. Phys. Lett.* **2002**, *360*, 534−542.
(45) Yang, T. X.; Tsushima, S.; Suzuki, A. Quantum Mechanical and Molecular Dynamical Simulations on Thorium(IV) Hydrates in Aqueous Solution. *J. Phys. Chem. A* **2001**, *105*, 10439−10445.
(46) Tsushima, S. Hydrolysis and Dimerization of Th^{4+} Ion. *J. Phys. Chem. B* **2008**, *112*, 7080−7085.
(47) Tsushima, S.; Yang, T. X.; Mochizuki, Y.; Okamoto, Y. Ab Initio Study on the Structures of Th(IV) Hydrate and Its Hydrolysis Products in Aqueous Solution. *Chem. Phys. Lett.* **2003**, *375*, 204−212.
(48) Yang, T. X.; Tsushima, S.; Suzuki, A. The Water Exchange Mechanism in Thorium (IV) Hydrates as Studied by Quantum Chemical Methods. *J. Solid State Chem.* **2003**, *171*, 235−241.
(49) Chaboy, J.; Diaz-Moreno, S. Ab Initio X-ray Absorption Spectroscopy Study of the Solvation Structure of Th(IV), U(IV), and Np(IV) in Aqueous Solution. *J. Phys. Chem. A* **2011**, *115*, 2345−2349.
(50) Torapava, N.; Persson, I.; Eriksson, L.; Lundberg, D. Hydration and Hydrolysis of Thorium(IV) in Aqueous Solution and the Structures of Two Crystalline Thorium(IV) Hydrates. *Inorg. Chem.* **2009**, *48*, 11712−11723.
(51) Spezia, R.; Beuchat, C.; Vuilleumier, R.; D Angelo, P.; Gagliardi, L. Unravelling the Hydration Structure of ThX_4 (X = Br, Cl) Water Solutions by Molecular Dynamics Simulations and X-ray Absorption Spectroscopy. *J. Phys. Chem. B* **2012**, *116*, 6465−6475.
(52) Szabo, Z.; Toraishi, T.; Vallet, V.; Grenthe, I. Solution Coordination Chemistry of Actinides: Thermodynamics, Structure and Reaction Mechanisms. *Coord. Chem. Rev.* **2006**, *250*, 784−815.
(53) Erras-Hanauer, H.; Clark, T.; van Eldik, R. Molecular Orbital and DFT Studies on Water Exchange Mechanisms of Metal Ions. *Coord. Chem. Rev.* **2003**, *238*, 233−253.
(54) Vallet, V.; Macak, P.; Wahlgren, U.; Grenthe, I. Actinide Chemistry in Solution, Quantum Chemical Methods and Models. *Theor. Chem. Acc.* **2006**, *115*, 145−160.
(55) Wickleder, M. S.; Fourest, B.; Dorhout, P. K. Thorium. In *The Chemistry of the Actinide and Transactinide Elements*; Morss, L. R., Edelstein, N. M., Fuger, J., Eds.; Springer: New York, 2006; Vol. *1*, pp 52−160.
(56) Rollet, A.; Bessada, C.; Rakhmatoulline, A.; Auger, Y.; Melin, P.; Gailhanou, M.; Thiaudière, D. In Situ High Temperature NMR and EXAFS Experiments in Rare-Earth Fluoride Molten Salts. *C. R. Chim.* **2004**, *7*, 1135−1140.
(57) Bessada, C.; Rollet, A.; Rakhmatullin, A.; Nuta, I.; Florian, P.; Massiot, D. In Situ NMR Approach of the Local Structure of Molten Materials at High Temperature. *C. R. Chim.* **2006**, *9*, 374−380.
(58) Meaker, R. E.; Porter, B.; Kesterke, D. G. *Electrical Conductivity and Density of Fluoride Systems*; US Dept. of Interior, Bureau of Mines: Washington, DC, 1971; Vol. *7528*.
(59) Castiglione, M. J.; Madden, P. A. Fluoride Ion Disorder and Clustering in Superionic PbF2. *J. Phys.-Condens. Mater.* **2001**, *13*, 9963−9983.
(60) Kashyap, H. K.; Annapureddy, H. V. R.; Raineri, F. O.; Margulis, C. J. How is Charge Transport Different in Ionic Liquids and Electrolyte Solutions? *J. Phys. Chem. B* **2011**, *115*, 13212−13221.
(61) Brown, E. A.; Porter, B. *Electrical Conductivity and Density of Molten Systems of Uranium Tetrafluoride and Thorium Fluoride with Alkali Fluorides*; US Dept. of Interior, Bureau of Mines: Washington, DC, 1964; Vol. *6500*.
(62) Gong, Y.; Hu, H.; Tian, G.; Rao, L.; Li, J.; Gibson, J. K. A Tetrapositive Metal Ion in the Gas Phase: Thorium(IV) Coordinated by Neutral Tridentate Ligands. *Angew. Chem., Int. Ed.* **2013**, *52*, 6885−6888.
(63) Mayer, I. Charge, Bond Order and Valence in the ab Initio SCF Theory. *Chem. Phys. Lett.* **1983**, *97*, 270−274.
(64) Gopinathan, M. S.; Jug, K. Valency. I. A Quantum Chemical Definition and Properties. *Theoret. Chim. Acta* **1983**, *63*, 497−509.
(65) Michalak, A.; DeKock, R. L.; Ziegler, T. Bond Multiplicity in Transition-Metal Complexes: Applications of Two-Electron Valence Indices. *J. Phys. Chem. A* **2008**, *112*, 7256−7263.
(66) Rabani, E.; Gezelter, J. D.; Berne, B. J. Calculating the Hopping Rate for Self-Diffusion on Rough Potential Energy Surfaces: Cage Correlations. *J. Chem. Phys.* **1997**, *107*, 6867−6876.
(67) Truhlar, D. G.; Hase, W. L.; Hynes, J. T. Current Status of Transition-State Theory. *J. Phys. Chem.* **1983**, *87*, 2664−2682.
(68) Masia, M.; Rey, R. Reaction Rate Theory Approach to Thermodynamic State Dependence of Hydration Shell Exchange for Li^+(aq). *J. Phys. Chem. B* **2003**, *107*, 2651−2659.
(69) Ozkanlar, A.; Clark, A. E. Chemnetworks: A Complex Network Analysis Tool for Chemical Systems. *J. Comput. Chem.* **2014**, *35*, 495−505.